

CONSTRAINTS ON PLANETARY COMPANIONS IN THE MAGNIFICATION $A = 256$ MICROLENSING EVENT:
OGLE-2003-BLG-423 *

JAIYUL YOO¹, D.L. DEPOY¹, A. GAL-YAM^{2,3}, B.S. GAUDI⁴, A. GOULD¹, C. HAN^{1,5}, Y. LIPKIN⁶, D. MAOZ⁶, E.O. OFEK⁶,
B.-G. PARK⁷, AND R.W. POGGE¹
(THE μ FUN COLLABORATION)

AND

M.K. SZYMAŃSKI⁸, A. UDALSKI⁸, O. SZEWCZYK⁸, M. KUBIAK⁸, K. ŻEBRUŃ⁸, G. PIETRZYŃSKI^{8,9}, I. SOSZYŃSKI⁸, AND
Ł. WYRZYKOWSKI^{8,6}
(THE OGLE COLLABORATION)

accepted for publication in The Astrophysical Journal

ABSTRACT

We develop a new method of modeling microlensing events based on a Monte Carlo simulation that incorporates both a Galactic model and the constraints imposed by the observed characteristics of the event. The method provides an unbiased way to analyze the event especially when parameters are poorly constrained by the observed lightcurve. We apply this method to search for planetary companions of the lens in OGLE-2003-BLG-423, whose maximum magnification $A_{\max} = 256 \pm 43$ (or $A_{\max} = 400 \pm 115$ from the lightcurve data alone) is the highest among single-lens events ever recorded. The method permits us, for the first time, to place constraints directly in the planet-mass/projected-physical-separation plane rather than in the mass-ratio/Einstein-radius plane as was done previously. For example, Jupiter-mass companions of main-sequence stars at 2.5 AU are excluded with 80% efficiency.

Subject headings: Galaxy: bulge — gravitational lensing — planetary systems — stars: low-mass, brown dwarfs

1. INTRODUCTION

High-magnification microlensing events are exceptionally sensitive to the presence of planetary companions to the lens. As the projected separation of the source and the (parent-star) lens decreases, the size of the images increases, thus enhancing the probability that the planet will pass close enough to an image to generate a noticeable deviation in the lightcurve (Gould & Loeb 1992). And if the source gets sufficiently close to the lens, the lightcurve can be perturbed by the central caustic associated with the parent star itself (Griest & Safizadeh 1998). Groups that monitor microlensing events to search for planets are well aware of this enhanced sensitivity and so devote special attention to these events.

It is therefore somewhat surprising that the vast majority of events monitored by these groups in the past have not

been particularly high-magnification, and the vast majority of the observations of the few that did reach high magnification were actually performed well away from the peak, when the event had far less sensitivity to planets. In particular, of the 43 events monitored by the PLANET (Probing Lensing Anomalies NETwork) collaboration (Albrow et al. 2001; Gaudi et al. 2002) over 5 years, most of the sensitivity to planets came from just 5 or 6 events, and most of that from the near-peak regions of these events. Tsapras et al. (2003) and Snodgrass et al. (2004) used the relatively sparse OGLE data to put limits on planetary systems, although Gaudi & Han (2004) have argued that planets could not be reliably detected from such data alone.

The main reason for this apparent discrepancy was simply a shortage of microlensing alerts. Hence, at any given time, there just were no high-magnification events in progress, or at least none near their peak. The available telescope time then had to be applied to less favorable events. In addition, when devising their observational strategy, PLANET considered that they would have to characterize the events they were monitoring entirely with their own data. Such characterization is absolutely essential to evaluating the sensitivity of each event to planets, and it requires a very large number of observations on the wings and at baseline when the event has very little sensitivity to planets.

With the commencement of the Optical Gravitational Lens Experiment's OGLE-III project (Udalski et al. 2002), the situation is radically changed. Using its dedicated 1.3 m telescope, large-format ($35' \times 35'$) camera, generally excellent seeing, and ambitious observing strategy, OGLE-III is alerting microlensing events toward the Galactic bulge at a rate of 500 per season. Since microlensing events are uniformly distributed in impact parameter u_0 , and since peak magnification scales $A_{\max} \sim u_0^{-1}$ (for $u_0 \ll 1$), this implies that there are dozens of events with $A_{\max} \gtrsim 10$ each year, and a handful

*BASED IN PART ON OBSERVATIONS OBTAINED WITH THE 1.3 M WARSAW TELESCOPE AT THE LAS CAMPANAS OBSERVATORY OF THE CARNEGIE INSTITUTION OF WASHINGTON.

¹ Department of Astronomy, The Ohio State University, 140 West 18th Avenue, Columbus, OH 43210; jaiyul, depoy, gould, pogge@astronomy.ohio-state.edu

² Department of Astronomy, California Institute of Technology, Pasadena, CA 91025; avishay@astro.caltech.edu

³ Hubble Fellow

⁴ Harvard-Smithsonian Center for Astrophysics, Cambridge, MA 02138; sgaudi@cfa.harvard.edu

⁵ Department of Physics, Institute for Basic Science Researches, Chungbuk National University, Chongju 361-763, Korea; cheongho@astroph.chungbuk.ac.kr

⁶ School of Physics and Astronomy and Wise Observatory, Tel Aviv University, Tel Aviv 69978, Israel; yiftah, dani, eran, lukas@wise.tau.ac.il

⁷ Korea Astronomy Observatory, 61-1, Whaam-Dong, Youseong-Gu, Daejeon 305-348, Korea; bgpark@boao.re.kr

⁸ Warsaw University Observatory, Al. Ujazdowskie 4, 00-478 Warszawa, Poland; msz, udalski, szewczyk, mk, zebrun, pietrzym, soszynsk, wyrzykow@astrouw.edu.pl

⁹ Departamento de Física, Universidad de Concepcion, Casilla 160-C, Concepcion, Chile

with $A_{\max} \gtrsim 100$. Moreover, OGLE-III photometry is publicly available (literally hours after it is taken), so there is generally no need for microlensing followup groups to monitor the wings or baseline in order to characterize the event. That is, followup observing time can be concentrated on the highly sensitive peaks of the high-magnification events. In the 2003 season, such peaks were occurring almost continuously. OGLE-III is therefore generating substantial new opportunities for microlensing planet search groups such as PLANET (Albrow et al. 1998), the Microlensing Planet Search (MPS, Rhie et al. 1999, 2000), and the Microlensing Follow-Up Network (μ FUN, Yoo et al. 2004).

However, the OGLE-III approach also generates substantial challenges. In order to monitor a very large area during the 2002 and 2003 seasons, OGLE-III returned to each field only of order 50 times over the roughly 9 month season. During the long nights around 21 June, when the bulge transits near midnight, the cadence was relatively high, once every two or three nights. But at the edges of bulge season, the rate of return dropped as low as once per week or less. Hence, some extremely high magnification events appeared quite ordinary as of their last observation before peak, and then could be recognized for what they were only very close to (or past) their peak. Indeed, it is quite possible that their true nature as high magnification events could not be recognized at all from the OGLE-III lightcurve alone. Thus, without additional work, the riches generated by OGLE-III could easily pass by unnoticed. Beginning in the 2004 season, OGLE adjusted its strategy to concentrate on a reduced number of fields that have relatively higher expected event rates. Hence, it is expected that the above-mentioned problems will be mitigated in future seasons.

Here we develop a new method of modeling microlensing events that incorporates both a Galactic model via a Monte Carlo simulation and the constraints imposed by the observed characteristics of the event. We apply this method to the extreme microlensing event (EME) OGLE-2003-BLG-423, which at $A_{\max} \sim 250$, proves to have the highest magnification ever recorded among single-lens events. As such, the event also has the greatest potential sensitivity to planetary companions of the lens, with substantial probability of detecting even Neptune mass planets, whose event timescale would typically be only about 6 hours. This enhanced sensitivity poses special challenges to the analysis because both the form and amplitude of the impact of such small planets on the lightcurve will depend on the relative size of the source compared to the Einstein ring. If this relative size were known, it would be straightforward to calculate its effect. However, since the lightcurve is consistent with a point source, our information on the source size is limited.

Similarly, using the lightcurve data alone the impact parameter u_0 is measured only to about 30%. If u_0 were known much more precisely (as it often is for events with relatively bright sources), then we would be able to specify with equal precision where in relation to the Einstein ring a planet could be and still avoid detection. With our less perfect knowledge of u_0 , however, we must be satisfied with a more probabilistic statement about these locations.

Both of these challenges are likely to be generic to the analysis of EMEs. Because such events occur with low probability, their sources are most likely to be the relatively common main-sequence stars that normally lie unnoticed in ground-based bulge images, but which can briefly leap to prominence in an EME. Since these main-sequence stars are

faint and hence small, they will most often avoid finite-source effects even in EMEs. Their faintness also induces large photometric errors in the wings of the lightcurve, the region that must be well-measured to accurately determine u_0 . For similar reasons, these two challenges are likely to be key issues in future, even more aggressive, microlensing experiments that aim to detect Earth-mass planets either by space-based (Bennett & Rhie 2002) or ground-based (Gaudi, Han & Gould 2004) observations.

In our analysis, we will take as our starting point the method pioneered by Gaudi & Sackett (2000) and Albrow et al. (2000), which was then applied to a much larger sample by Gaudi et al. (2002). However, we improve upon this method in several respects. First, we fix the impact parameter u_0 at a series of different values consistent with the event data and evaluate the sensitivity to companions at each u_0 . To find the net sensitivity, we must weight each of these outcomes by the relative probability that the actual event had that particular u_0 . Second, we determine these relative probabilities not just from the fit to the lightcurve data, but by incorporating the results of a Monte Carlo simulation of events toward the actual line of sight. For each trial u_0 , we weight the simulated events by how well they reproduce both the observed characteristics of the lightcurve and the probability that the source has the luminosity inferred from the lightcurve combined with the Monte Carlo event parameters, as determined from the Hipparcos luminosity distribution at the observed color of the source. This method not only allows us to more accurately estimate the planetary sensitivity, it also permits us to characterize this sensitivity as a function of planet mass and planet-star separation, since each simulated event has a definite lens mass (drawn from the adopted mass function) and definite lens and source distances (and so definite Einstein radius). In contrast, the original approach of Albrow et al. (2000) yielded sensitivities in terms of two lightcurve-fit parameters, the planet-star mass ratio and the separation in units of the Einstein radius.

This method would also permit a similarly rigorous statistical treatment of finite source effects, since each simulated event has a definite ratio of source size to Einstein radius. However, based on the Monte Carlo, we show that in the case of OGLE-2003-BLG-423, finite-source effects are negligible.

2. DATA

OGLE-2003-BLG-423 was alerted by the Early Warning System (EWS, Udalski 2003) on UT 7:38 14 Sept 2003, almost exactly 24 hours before the peak on $HJD' \equiv HJD - 2450000 = 2897.8070$, and less than 5 hours after the triggering observation by the OGLE-III observatory in Las Campanas, Chile. While the automated alert did not itself call any more attention to this event than the other three that were alerted simultaneously, the OGLE web site¹⁰ immediately affixed a “!” to this event, indicating that it was of special interest. Moreover, from the data available at the web site one could see that the event was already 3 mag above baseline and rising rapidly. See Albrow (2004) for a Bayesian approach to determine whether ascending microlensing events are likely to achieve high magnification.

Immediately following the alert, μ FUN decided to focus its observations heavily upon this event. Because the event was triggered relatively late in the season when the bulge is already west of the meridian at twilight, the time per night that it could be observed from any one site was restricted: roughly

¹⁰ <http://www.astrouw.edu.pl/~ogle/ogle3/ews/ews.html>

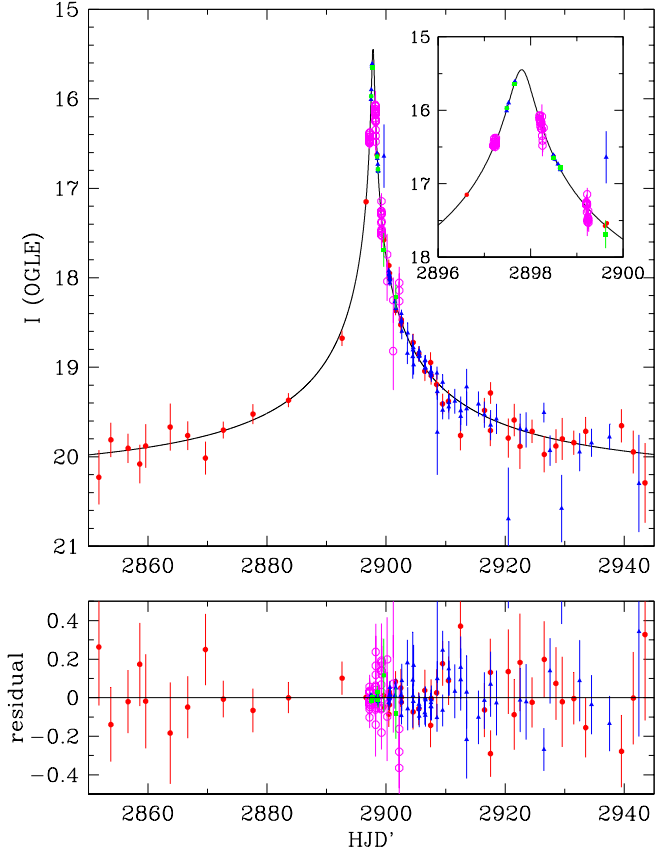


FIG. 1.— Lightcurve of microlensing event OGLE-2003-BLG-423 near its peak on 15 Sep 2003 (HJD 2452897.8070). Data points with 1σ error bars are in I (OGLE: red filled circles; μ FUN Chile: blue filled triangles; μ FUN Israel: magenta open circles) and V (μ FUN Chile: green filled squares). All bands are linearly rescaled so that F_s and F_b are the same as the OGLE observations, which define the magnitude scale. The solid curve shows the best-fit point-source/point-lens model for the I -band curve.

1.5 hours from the Wise Observatory in Israel and roughly 4 hours from CTIO at La Serena, Chile. The gap in coverage between the two observatories was about 6 hours. Because of a communication error, the Chile observations have a gap of 3 hours the first night, but are then generally spaced at roughly 1 hour intervals on subsequent nights.

While OGLE-III normally cycles through many fields (survey mode), it can also operate in followup mode when there is an event of particular interest. OGLE-2003-BLG-423 was immediately designated as such an event, but because of communication problems, it was not observed the first night following discovery. However, it was observed one to four times per night over the next five nights.

When combined, observations from these three observatories provide reasonably good coverage of the peak. See Figure 1. The μ FUN data are available at the μ FUN web site¹¹ and the OGLE data are available at the above-mentioned OGLE EWS web site.

From a fit to the first two nights of μ FUN observations, it was already clear that the effective timescale of the event was very short, $t_{\text{eff}} \equiv u_0 t_E = 0.24$ day, where t_E is the Einstein crossing time and u_0 is the impact parameter in units of

the Einstein radius. Combining this with the Einstein crossing time $t_E = 97$ days derived from the OGLE data yielded an estimate of $A_{\text{max}} \simeq 1/u_0 \sim 400$, which would be the highest magnification single-lens event ever recorded. Recognizing the importance of this event, OGLE and μ FUN worked together to develop an observation plan that would allow us to characterize it as well as possible. Our principal concern was that if OGLE returned to its regular cycle of observations and μ FUN stopped observing the event altogether (as both would normally do several days after the peak), then the OGLE and μ FUN observations might barely overlap in time, meaning that the two photometry systems could not be rigidly linked into a single lightcurve. To resolve this problem, we agreed to each observe the event several times for the next few nights (weather permitting) and to both regularly continue observing it until it got too close to the Sun.

There are a total of 278 I band images including 150 from OGLE, 78 from μ FUN Chile, and 50 from μ FUN Israel. In addition there are 7 V band images from μ FUN Chile, all taken near peak for the purpose of determining the color of the source. Finally, since μ FUN Chile observations are carried out with an optical/infrared camera, all V and I images from this location are automatically accompanied by H band images. However, even at peak, the event was too faint in H for these observations to be useful. For each data set, the errors were rescaled to make χ^2 per degree of freedom for the best-fit point-source/point-lens (PSPL) model equal to unity. We then eliminated the largest outlier and repeated the process until there were no 3σ outliers. This resulted in the elimination of 1 OGLE point, 1 μ FUN Chile I point and 1 μ FUN V point. In the neighborhood of each of these four outliers, there are other data points that agree with the PSPL model, showing that the outliers are indeed caused by systematic errors rather than revealing unmodeled structure in the lightcurve. The final rescaling factors were 1.13 and 0.82 for OGLE and μ FUN Chile I , respectively. The other two observatory/filter combinations did not require renormalization. The descriptions of the instruments, observing protocol, and reduction procedures are identical to those given in Yoo et al. (2004). The photometry is carried out using the DoPHOT-based PLANET pipeline.

3. POINT-LENS MODELS

The signature of a planetary companion will usually be a brief excursion from an otherwise “normal” point-lens magnification lightcurve. Indeed, as outlined by Gould & Loeb (1992), it is often possible to estimate the planet’s properties from the gross characteristics of this deviation. The first step to searching for planets is therefore to fit the lightcurve to a point-lens model (Albrow et al. 2000). However, planetary deviations can be strongly affected by the finite size of the source, even if the rest of the lightcurve is perfectly consistent with a point source, which can lead to degeneracies in the interpretation of the deviation (Gaudi & Gould 1997), or even to a complete failure to detect the deviation. Hence, we begin by presenting the best-fit PSPL model, and then investigate to what extent finite-source effects can be detected or constrained within the context of point-lens models.

3.1. Point-Source Point-Lens Model

We fit the data to PSPL models, defined by three lensing geometry parameters (t_0 , u_0 , and t_E) as well as a source flux F_s and a blended-light flux F_b for each observatory-filter com-

¹¹ <http://www.astronomy.ohio-state.edu/~microfun>

TABLE 1. OGLE-2003-BLG-423 FIT PARAMETERS

	Lightcurve Alone						Lightcurve & Monte Carlo Simulation					
	t_0 (days)	u_0	t_E (days)	A_{\max}	I_s	I_{base}	t_0 (days)	u_0	t_E (days)	A_{\max}	I_s	I_{base}
Value	2897.8070	0.00250	97.4	400	22.0	20.21	2897.8070	0.00391	62.1	256	21.47	20.21
Error	0.0030	0.00072	27.9	115	0.3	0.03	0.0030	0.00066	10.5	43	0.08	0.03

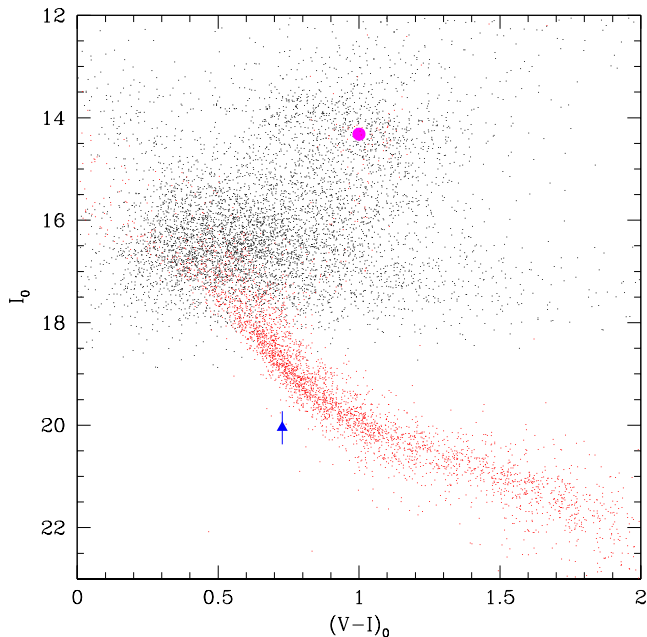


FIG. 2.— Instrumental CMD of a 6′ square around OGLE-2003-BLG-423, which has been converted to dereddened magnitude and color by translating the centroid of the clump giants (magenta circle) to its known position $[I_0, (V-I)_0]_{\text{clump}} = (1.00, 14.32)$. Hipparcos main sequence stars placed at $R_0 = 8$ kpc are represented as red points. The source (blue triangle with 1 σ errorbar) is significantly fainter than the Hipparcos stars.

bination i . That is,

$$F_i(t) = F_{s,i}A[u(t)] + F_{b,i}, \quad A(u) = \frac{u^2 + 2}{u\sqrt{u^2 + 4}}, \quad (1)$$

where $[u(t)]^2 = u_0^2 + (t - t_0)^2/t_E^2$. The best-fit parameters and their errors as determined from the lightcurve data alone are shown in Table 1 (also see Fig. 1). In Table 2, we present flux-parameters from the lightcurve alone that are rescaled to be the same as in the OGLE I -band photometry. We find that even though the event is quite long, the source is too faint to detect microlensing parallax effects.

There are several notable features of this fit. First, the impact parameter is extremely small, $u_0 = 0.00250 \pm 0.00072$ implying that the maximum magnification is $A_{\max} = 400 \pm 115$. Second, the source is extremely faint, $I_s = 22.0 \pm 0.3$. The OGLE photometry is not rigorously calibrated, but is believed to be accurate to a few tenths. Finally, the errors are quite large, roughly 30% for each of t_E , u_0 , and F_s . In fact, these errors are extremely correlated: appropriate combinations of these parameters, $t_{\text{eff}} \equiv u_0 t_E$ and $F_{\max} \equiv F_s/u_0$, have much smaller errors,

$$t_{\text{eff}} = 0.2429 \pm 0.0037 \text{ days}, \quad I_{\min} = 15.459 \pm 0.018. \quad (2)$$

TABLE 2. OGLE-2003-BLG-423 FLUXES PARAMETERS (LIGHTCURVE ALONE)

	OGLE-I	μ FUN-I Chile	μ FUN-I Israel	μ FUN-V Chile
f_s	0.02596	0.02596	0.02596	0.02596
σ_{f_s}	0.00754	0.00745	0.00744	0.00745
f_b	0.10411	0.02396	-0.23491	0.36952
σ_{f_b}	0.00607	0.00484	0.05733	0.08673

NOTE. — f_s is rescaled to be the same as in the OGLE-I photometry

3.2. Color-Magnitude Diagram

The first step to understanding the impact of these measurements and their errors is to place the source on an instrumental color-magnitude diagram (CMD). In Figure 2, we have translated the instrumental CMD to place the clump at $[(V-I)_0, I_0] = (1.00, 14.32)$, which is the dereddened color and absolute magnitude of the Hipparcos (ESA 1997) clump when placed at the Galactocentric distance, $R_0 = 8$ kpc (Yoo et al. 2004). The source position (as determined from the model fit) is shown as a triangle. Since the source is substantially fainter than any of the CMD stars, we also plot the Hipparcos lower main sequence in the figure (also placed at R_0). Note that the source has a dereddened color $(V-I)_0 = 0.73$, almost exactly the same as the Sun. The instrumental source color (and so the source color relative to the clump) is not model dependent: it can be derived directly from a regression of V flux on I flux, without reference to any model. If the source suffers similar extinction as the clump, then the source is about 1.4 mag fainter than the Sun would be if placed at the distance to the clump, i.e., R_0 . The Sun is somewhat evolved off the main sequence, but the source is still more than 1 mag fainter than zero-age main-sequence stars of the same color and metallicity. This offset between the source and the main-sequence (placed at R_0) hardly changes even if one assumes a substantial difference between the source reddening and the mean reddening toward the clump stars because the reddening vector is nearly parallel to the main sequence.

There are basically only three effects that could contribute to this offset. First, the source actually could lie well behind the bulge. Second, the source could be relatively metal poor and so subluminal compared to solar-neighborhood stars. Third, the microlensing model could be in error, either statistically or systematically. We make a more detailed investigation on this offset in § 4.4.

3.3. Finite-Source Effects

We now explore a set of models that are constrained to hold u_0 and z_0 at a fixed grid of values. Here, $z_0 \equiv u_0/\rho_*$ and $\rho_* = \theta_*/\theta_E$ is the angular size of the source θ_* in units of the angular Einstein radius θ_E . We take account of limb darkening

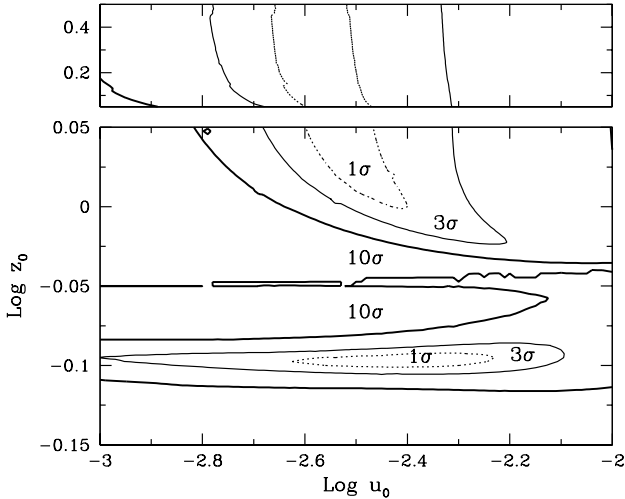


FIG. 3.— Likelihood contours relative to the best-fit point-source/point-lens model for various point-lens models with finite-source effects, where u_0 is the impact parameter, $z_0 \equiv u_0/\rho_*$, and ρ_* is the angular size of the source in units of the angular Einstein radius. Both top and bottom panels are linear in $\log z_0$, but differ in scale. As the source-lens separation increases ($z_0 \gtrsim 1$), the contours become independent of z_0 . Note the isolated minimum at $z_0 \simeq 0.8$.

by parameterizing the surface brightness S by,

$$\frac{S(\vartheta)}{S_0} = 1 - \Gamma \left[1 - \frac{3}{2}(1 - \cos \vartheta) \right], \quad (3)$$

where ϑ is the angle between the normal to the stellar surface and the line of sight. Since the source has almost exactly the color of the Sun, we assume solar values for Γ ,

$$\Gamma_V = 0.528, \quad \Gamma_I = 0.368. \quad (4)$$

Figure 3 shows $\Delta\chi^2$ contours for the various models plotted as functions of u_0 and z_0 . These contours are essentially independent of z_0 , for $z_0 \gtrsim 1$, i.e., for models in which the lens does not pass directly over the source. Note that although models with $z_0 \simeq 1$ are strongly excluded, there are some models with $z_0 \simeq 0.8$ that are permitted at the 1σ level.

Even though we cannot rule out the model at the isolated minimum ($u_0 \simeq 0.004$ and $z_0 \simeq 0.8$) based on the lightcurve data alone, it is extremely unlikely to describe the event if we take account of the observed properties of the event combined with a Galactic model (see § 4). For the moment, we therefore assume $z_0 > 1$ and ignore finite-source effects. Nevertheless, as we describe below, the process of recognizing an EME induces a strong selection bias toward large t_E events and so toward those with high θ_E and/or low relative proper motion μ . Hence, in § 4 we will investigate the possibility of $z_0 \lesssim 1$ more closely after we evaluate the posterior probability.

4. MODELING THE EVENT

We first outline a new method to analyze microlensing events that incorporates both a Galactic model via a Monte Carlo simulation and the constraints imposed by the observed characteristics of the event. This method is completely general and can be applied to any microlensing event. We then apply the method to OGLE-2003-BLG-423.

4.1. General Formalism

In most scientific experiments, ones seeks to determine the posterior probability $P(\mathbf{a}|\Delta)$ of a parameter set $\mathbf{a} = (a_1 \dots a_n)$ given a data set Δ . By Bayes' theorem,

$$P(\mathbf{a}|\Delta) = P_{rel}(\Delta|\mathbf{a})P_{pri}(\mathbf{a}), \quad (5)$$

where $P_{rel}(\Delta|\mathbf{a})$ is the probability of the data given the model parameters \mathbf{a} and $P_{pri}(\mathbf{a})$ is the prior probability of the parameters. For microlensing events,

$$P_{rel}(\Delta|\mathbf{a}^{lc}) = \exp[-\Delta\chi^2(\mathbf{a}^{lc})/2], \quad (6)$$

where \mathbf{a}^{lc} is the set of parameters describing the lightcurve and $\Delta\chi^2(\mathbf{a}^{lc})$ is the χ^2 difference relative to the best-fit model.

Since the prior $P_{pri}(\mathbf{a}^{lc})$ is often assumed to be uniform, minimization of $\chi^2(\mathbf{a}^{lc})$ is the usual method to find a best parameter set \mathbf{a}^{lc} . This procedure is appropriate when the lightcurve tightly constrains the parameters, but in general it is more correct to take account of the priors. However, the priors on some of the lightcurve parameters \mathbf{a}^{lc} cannot be directly specified. While u_0 and t_0 can be taken as random variables drawn from uniform distributions, t_E is a function of several independent physical quantities, namely the lens mass, the distances to the lens and source, and the transverse velocities of the lens and source. We collectively denote these independent physical parameters as \mathbf{a}^{phys} . Therefore, Bayes' theorem can be rewritten,

$$P(\mathbf{a}^{lc}, \mathbf{a}^{phys}|\Delta) = \exp[-\Delta\chi^2(\mathbf{a}^{lc})/2]P_{pri}(\mathbf{a}^{lc}, \mathbf{a}^{phys}), \quad (7)$$

where it is understood that some of the lightcurve parameters are determined by the physical parameters. At the end of the day, one may be more interested in the physical parameters (or some subset of them) than the lightcurve parameters, and so after obtaining the general probability distribution given by equation (7), one may integrate over the remaining “nuisance parameters” to get the probability distribution of a specific physical parameter. Indeed, we will do exactly this when we evaluate planet sensitivities in § 6.2.

4.2. Relative Likelihood

To apply this general method to OGLE-2003-BLG-423, we first simplify $\Delta\chi^2(\mathbf{a}^{lc})$. In principle, $\Delta\chi^2$ is a function of all five parameters, t_0, u_0, t_E, F_s , and F_b . In practice, t_0 is extremely well determined from the data, while the remaining four parameters are all highly correlated. That is, since $t_{eff} = u_0 t_E$ and $F_{max} = F_s/u_0$ (and so I_{min}) are very well determined from the lightcurve data (see eq. [2]), their product $F_{max} t_{eff} = F_s t_E$ is also well determined. Moreover, since the baseline flux is well determined, F_s and F_b are almost perfectly anti-correlated. Hence, once t_E is chosen in a particular Monte Carlo realization, I_s is also fixed to within 0.008 mag and all other parameters are rigidly fixed as well. Therefore, the relative likelihood is,

$$\exp[-\Delta\chi^2(\mathbf{a}^{lc})/2] = \exp[-\Delta\chi^2(t_E)/2], \quad (8)$$

where $\Delta\chi^2(t_E)$ is the χ^2 difference relative to the best-fit PSPL model. Since all of the lightcurve parameters are determined from the physical parameters via the well-constrained lightcurve parameters t_0, t_{eff} , and F_{max} , Bayes' theorem can be rewritten in our case,

$$P(\mathbf{a}^{phys}|\Delta) = \exp[-\Delta\chi^2(t_E(\mathbf{a}^{phys}))/2]P_{pri}(\mathbf{a}^{phys}). \quad (9)$$

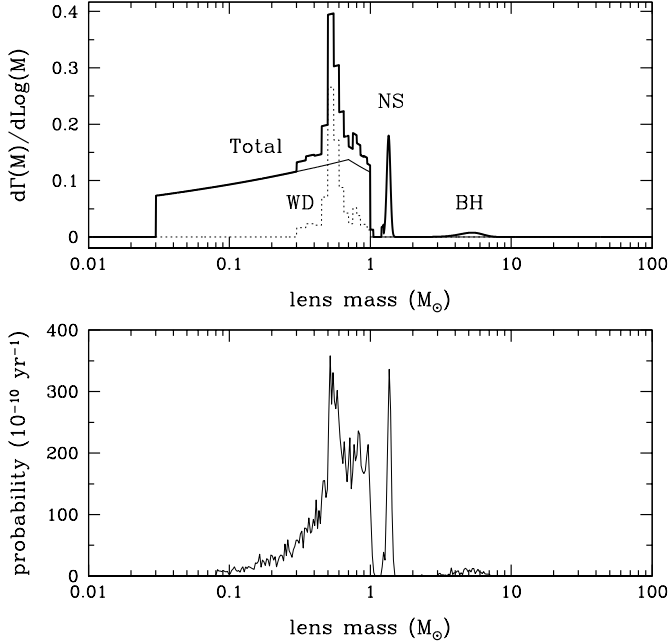


FIG. 4.— Microlensing event rate toward the Galactic bulge as a function of mass. The upper panel shows event rates for main sequence stars and brown dwarfs (*thin solid line*) and for white-dwarf, neutron-star, and black-hole remnants (*dotted line*). The total event rate is shown as a thick solid line (see Gould 2000). The lower panel shows the posterior probability of the Monte Carlo events that takes account of both a Galactic model and the Hipparcos-based luminosity distribution at the observed source color.

4.3. Prior Probability

In order to estimate the prior probability $P_{pri}(\mathbf{a}^{\text{phys}})$, we Monte Carlo the event, considering all combinations of source and lens distances, $D_l < D_s$, uniformly sampled along the line of sight toward the source $(l, b) = (0.4961, -5.1775)$. We choose a lens mass randomly from the Gould (2000) bulge mass function, and use Gaussian random variables to assign each component of the transverse velocities \mathbf{v}_\perp of the lens and source. Although this mass function is strictly valid only for the bulge, it should be approximately valid for the disk as well. This is because at $b = -5.2$, the line of sight generally passes more than a scale height below the Galactic plane, where the stars are older (and therefore more bulge-like) than they are in the immediate solar neighborhood, where the disk mass function is best measured. The event rate for this Monte Carlo realization is then,

$$\Gamma \propto \rho_{\text{HG}}(D_s) D_s^2 \rho_{\text{HG}}(D_l) D_l^2 \theta_E \mu, \quad (10)$$

where the density ρ_{HG} as well as the lens and source velocity distribution are as given by the Han & Gould (1996, 2003) model. The parameters

$$\mu \equiv |\boldsymbol{\mu}_s - \boldsymbol{\mu}_l| = \left| \frac{\mathbf{v}_{\perp,s}}{D_s} - \frac{\mathbf{v}_{\perp,l}}{D_l} \right|, \quad (11)$$

$$\theta_E \equiv \sqrt{\frac{4GM}{c^2} \left(\frac{1}{D_l} - \frac{1}{D_s} \right)},$$

and $t_E = \theta_E/\mu$, are all fixed by the chosen distances, transverse velocities, and mass. While this Galactic model is not a perfect representation of the Galaxy, it is substantially more accurate than the uniform prior distribution normally assumed in most microlensing analyses.

We next impose another condition on the prior that constrains \mathbf{a}^{phys} . Since t_E is fixed by the Monte Carlo, F_s is also fixed (see § 4.2). By comparing this to the position of the clump on the instrumental CMD, one can then determine the dereddened flux of the source. Since D_s is fixed by the Monte Carlo, the absolute magnitude of the source for this Monte Carlo realization can also be inferred. The prior probability is then proportional to N_{Hip} , the number of Hipparcos stars with this inferred absolute magnitude (and within 0.02 mag of the measured source $V-I$ color). Hence, if we restrict attention to the k -th realization of the Monte Carlo with physical parameters $\mathbf{a}^{\text{phys},k}$, the prior probability is given by,

$$P_{pri}(\mathbf{a}^{\text{phys},k}) \propto (\Gamma N_{\text{Hip}})_k. \quad (12)$$

4.4. Posterior Probability

Combining equations (9) and (12) implies that the posterior probability that a parameter a_i lies in the interval $a_i \in [a_{i,\text{min}}, a_{i,\text{max}}]$ is proportional to,

$$P(a_i \in [a_{i,\text{min}}, a_{i,\text{max}}]) \propto \sum_k P(\mathbf{a}^{\text{phys},k}), \quad (13)$$

where

$$P(\mathbf{a}^{\text{phys},k}) = (\Gamma N_{\text{Hip}})_k \exp[-\Delta\chi^2(t_{E,k})/2] \times \Theta(a_i(\mathbf{a}^{\text{phys},k}) - a_{i,\text{min}}) \Theta(a_{i,\text{max}} - a_i(\mathbf{a}^{\text{phys},k})), \quad (14)$$

a_i is one of the physical parameters \mathbf{a}^{phys} (or possibly a function of several physical parameters as would be the case for $a_i \in \mathbf{a}^{\text{lc}}$), both $(\Gamma N_{\text{Hip}})_k$ and $t_{E,k}$ are implicit functions of $\mathbf{a}^{\text{phys},k}$, and Θ is a step function.

Letting $a_i = M$, we can evaluate the posterior probability distribution for the lens mass. Figure 4 shows both the event rate Γ and the posterior distribution of microlensing events toward the Galactic bulge as a function of mass. The overall event rate is shown in the upper panel. The thin solid and dotted lines represent events from MS stars and brown dwarfs (BDs), and from stellar remnants, respectively. Note that the number of objects in the mass function steeply decreases as the mass increases ($M > 0.7M_\odot$), and in particular that there are no MS stars of $M \gtrsim 1M_\odot$ in the Galactic bulge because such stars have already evolved off (Holtzman et al. 1998; Zoccali et al. 2000). However, since the cross-section of the microlensing event is proportional to $M^{1/2}$, remnants contribute of order 20% of the bulge microlensing events (Gould 2000). The posterior distribution for the lens mass is shown in the lower panel. Note that high masses are strongly favored, possibly because of the long timescale t_E .

Figure 5 shows the distributions of posterior probabilities of various other parameters. The thick and thin solid histograms represent bulge-bulge and disk-bulge events, respectively. The upper left panel shows the distribution of impact parameters (*histograms*) compared to the distribution derived from the lightcurve data alone (*solid curve*). Note that the best-fit u_0 from the lightcurve alone is somewhat lower than the peak of the posterior distribution (see § 6). The impact parameter and the apparent magnitude are strongly anticorrelated as is discussed in § 3.1, and the lower left panel shows the distribution of source dereddened apparent magnitudes (*histograms*) compared to the distribution based on the lightcurve data alone (as represented by the solid curve in Fig. 5 and by the position and error bar in Fig. 2). Taking account of the prior probabilities Γ of the Galactic model and of the M_l distribution of Hipparcos stars at the observed source

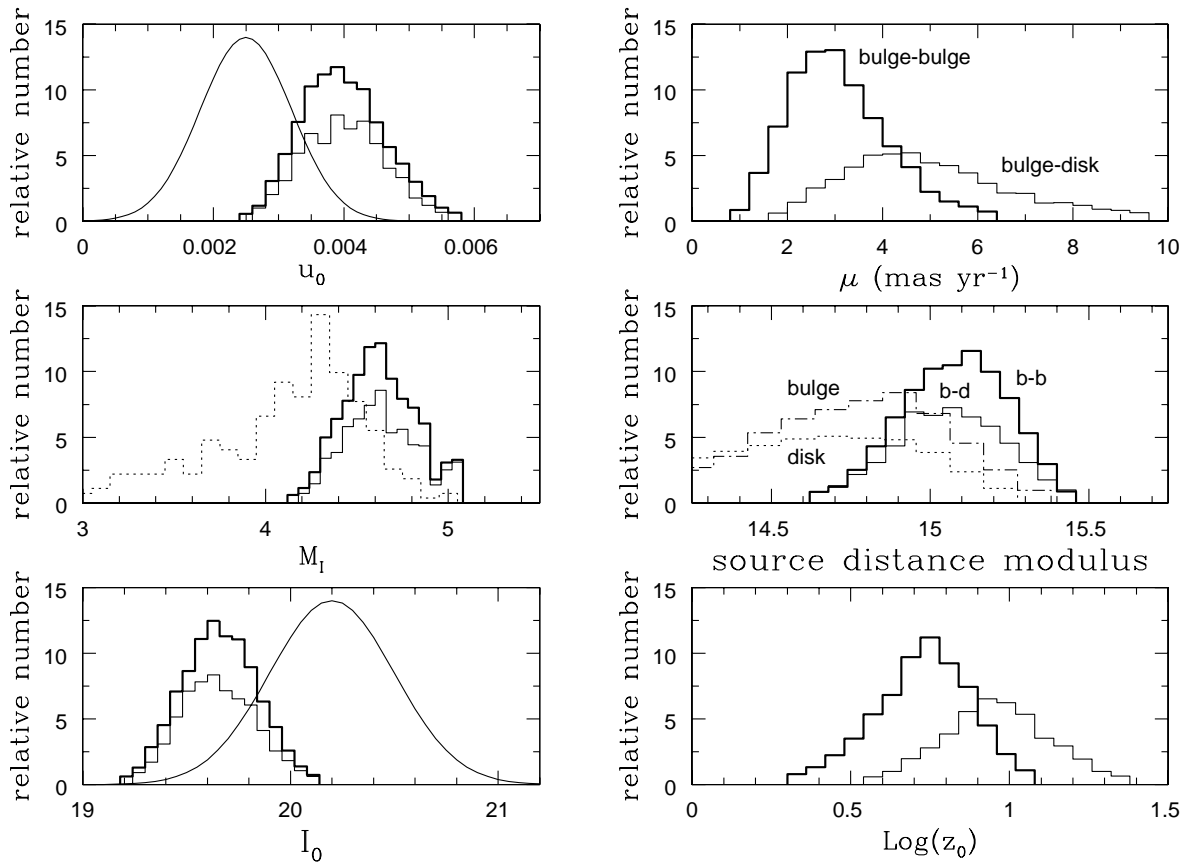


FIG. 5.— Distributions of Monte Carlo microlensing events toward the OGLE-2003-BLG-423 line of sight. The thick and thin solid lines represent bulge-bulge events and bulge-disk events, respectively. The impact parameter, absolute magnitude, dereddened apparent magnitude, and source-lens relative proper motion are denoted as u_0 , M_I , I_0 , and μ , respectively, while $z_0 \equiv u_0/\rho_*$, where ρ_* is the ratio of the source size to the Einstein radius. The Gaussian curves in the u_0 and I_0 panels represent the probability distributions derived from the lightcurve fit alone, i.e., before applying the constraints from the Galactic model. The dotted histograms in the middle panels are the distributions of Hipparcos stars at the color of the source, $(V-I)_0 = 0.73$ (left panel), and lenses in the bulge and disk obtained from a Galactic model alone (right panel), respectively.

color $(V-I)_0 = 0.73$ drives the source to somewhat brighter apparent magnitudes, but it is still consistent with the result derived from the lightcurve data alone.

The dotted histogram in the middle left panel represents the absolute magnitude of Hipparcos MS stars with the same color as the source. However, the Monte Carlo events favored by the lightcurve are dimmer than the average Hipparcos star at R_0 (see the middle right panel). The lower right panel shows the distribution of z_0 . As we discuss in § 5, the Monte Carlo effectively takes account of the selection effects that push toward low proper motion (and hence lower z_0). The panel shows, however, that the probability that z_0 is small enough to generate significant finite-source effects in a point-lens event is extremely small.

The best-fit lightcurve parameters and their errors are shown in Table 1. Note that parameters are different at the 2σ level from those with lightcurve alone, and hence the maximum magnification of the event is $A_{\max} = 256 \pm 43$.

5. INFLUENCE OF SELECTION EFFECTS

As mentioned in § 2, the event was alerted only 24 hours before peak. The observation just prior to this triggering observation was on 2892.6, about 4 days previous. The event was not alerted from that observation because up to that point there

were only two detections on the subtracted images, whereas the alert threshold is set at three in order to avoid spurious events. Even had the event been alerted, it would have been flagged as having an impact parameter $u_0 = 0.0 \pm 0.2$ and therefore would not have been recognized as a high magnification event. This 4-day cycle time, which was typical for OGLE-III observations in mid-September, introduces significant selection effects in the recovery of EMEs.

The primary effect is to select for long events. For example, if we consider an event with the same source star, same impact parameter, and same magnification on 2892.6, but with t_E shorter by a factor $2/3$, then it would not have been discovered until after peak. That is, such an event would also not have triggered an alert on 2892.6, but at the 2896.6 observation, at which point it would have already been 0.5 days past peak. By the time followup observations started, it would have been a day past peak, and so magnified only about 40 times. While still impressive, this would not have garnered either the attention or the intensive observations triggered by OGLE-2003-BLG-423.

Thus, the fact that the observed timescale is long compared to that of typical bulge microlensing events is explained largely by selection. However, this selection effect is already fully accounted for in the Monte Carlo. Consider a Monte

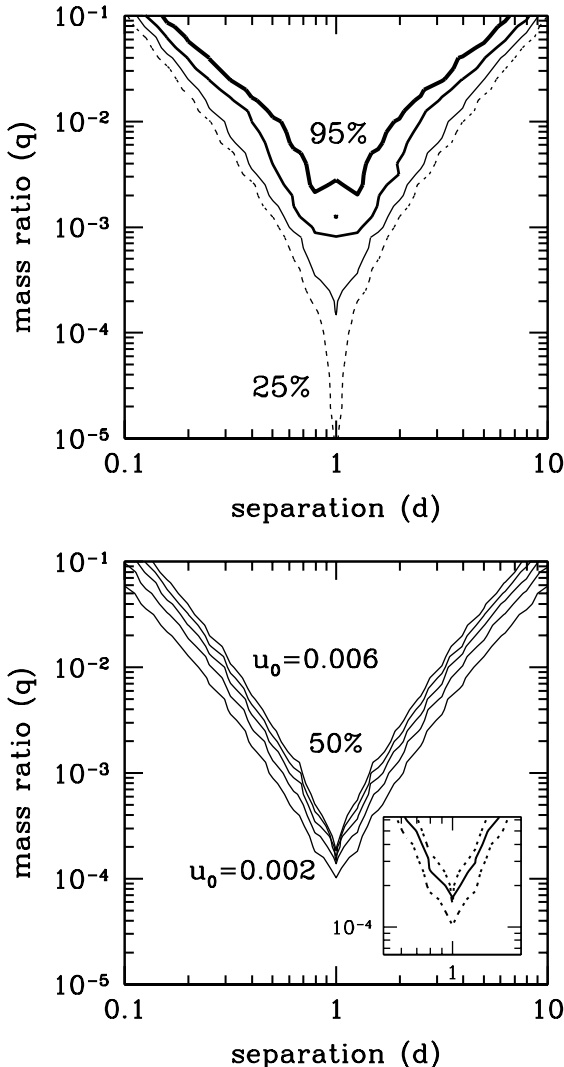


FIG. 6.— Detection efficiency of OGLE-2003-BLG-423 in units of planet-star mass ratio q and separation d (normalized to the Einstein radius). The upper panel shows the detection efficiency contours (25%, 50%, 75%, and 95%) by minimizing χ^2 with respect to t_0 , t_E , and u_0 (Albrow et al. 2000), and the lower panel shows the 50% efficiency contours for various fixed u_0 ($u_0 = 0.002$ to 0.006). As u_0 increases, the efficiency decreases monotonically. For comparison, we present the 50% contours of the former method (solid) and the latter method with $u_0 = 0.002, 0.004$ (dashed) in the inset.

Carlo event that has a t_E that is much shorter than the best fit in Table 1, say $t_E = 20$ days rather than 97 days. This event is assigned a source flux that is lower by a factor ~ 4.5 so as to reproduce as well as possible the observed lightcurve. In fact, the resulting model lightcurve reproduces the peak region extremely well: most of the χ^2 difference comes from the post-peak wing, which of course did not enter the selection process. Thus, there is no additional selection discrimination among the Monte Carlo events.

The event appears to have several “abnormal” characteristics relative to typical events as represented in the Monte Carlo, and it is of interest to determine which of these are brought about by, or enhanced by selection. The most likely source distance is about 2.5 kpc behind the Galactic center.

For bulge-bulge lensing, there is a general selection effect driving toward distant sources because these have larger θ_E and so larger cross sections. See equation (10). However, as shown by the dotted lines in the middle right panel of Figure 5, this effect alone pushes the peak of the distribution back only 1.5 kpc (0.7 kpc for bulge-disk lensing) relative to R_0 , not 2.5 kpc. The pressure toward longer events further selects for more distant sources because their larger θ_E make the events longer. However, since the FWHM of the prior distribution is about 3.5 kpc, the adopted distance would not be extremely unlikely in any case.

Another abnormal characteristic is the faintness of the source. Up to a point, the event selection procedure would appear to pick out brighter sources. As mentioned above, a brighter source would exactly compensate in the selection process for a shorter event, and these are more common than longer events. However, fainter sources are more common than brighter ones, and this is a larger effect. Moreover, as the source brightness increases, so does its angular size, and this eventually cuts off the peak brightness due to finite source effects. Based on Figure 5, however, we have concluded that the source is probably nowhere near this threshold, so this limitation on source size does not enter as a significant factor.

Finally, the source appears to be dim for its color. If the Hipparcos distribution is representative of bulge stars of solar color, then this feature would actually be selected against: more luminous stars would be both more numerous and, if lensed by exactly the same lens, more easily recognized before peak. However, it may be that the Hipparcos distribution is not representative of the bulge. For example, the stars in the outer bulge may have significantly lower metallicity than those in the solar neighborhood, and therefore be fainter at fixed color as is true of subdwarfs in the solar neighborhood (e.g., Gould 2004).

We conclude that while a number of the features of this event appear unusual at first sight, most are explained in whole or in part by selection effects.

6. SEARCH FOR PLANETS

6.1. Detection Efficiency

As discussed in § 1, Gaudi & Sackett (2000) and Albrow et al. (2000) have already developed a procedure for searching for planets in microlensing lightcurves, and Gaudi et al. (2002) have applied this to a sample of 43 events. For each event, they considered an ensemble of planetary systems characterized by a planet-star mass ratio q , a planet-star separation (in units of the Einstein radius) d , and an angle α of the source trajectory relative to the planet-star axis. We will begin by following this procedure, but will introduce several important modifications.

For a given (d, q) , we define the detection efficiency $\epsilon(d, q)$ as the probability that a companion planetary system described by (d, q) would have produced a lightcurve deviation inconsistent with the observed OGLE-2003-BLG-423 lightcurve:

$$\epsilon(d, q) = \frac{1}{2\pi} \int_0^{2\pi} d\alpha \Theta [\chi^2(d, q, \alpha) - \chi_{\text{PSPL}}^2 - \Delta\chi_{\text{thr}}^2], \quad (15)$$

where $\chi^2(d, q, \alpha)$ is the value of χ^2 evaluated for these three parameters, χ_{PSPL}^2 its best-fit value for the PSPL model, and Θ is a step function. The (d, q) sampling is 0.1 in the log, and the angular step size is set to be $\Delta\alpha = \sqrt{q}/2$ in order to avoid missing possible planetary perturbations. We choose a

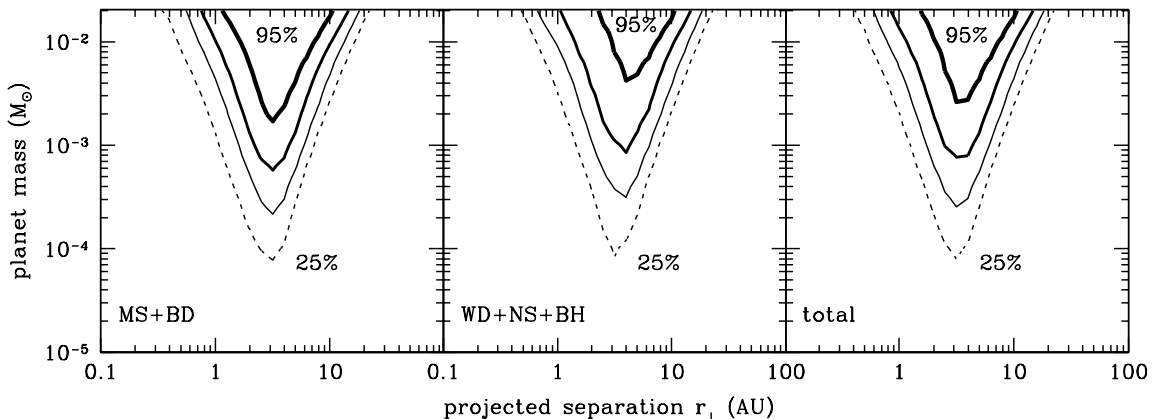


FIG. 7.— Convolved detection efficiency contours of OGLE-2003-BLG-423 as a function of the physical mass and the separation of the planetary companion. The efficiency contours from MS+BDs and remnants are shown separately in the left and central panels respectively, while the total is shown in the right panel. Contours represent $\epsilon = 25\%$, 50%, 75% and 95% efficiency.

conservative threshold, $\Delta\chi^2_{\text{thr}} = 60$ (Gaudi et al. 2002). In this incarnation of the procedure, we follow Albrow et al. (2000) and adopt for $\chi^2(d, q, \alpha)$ the minimum value of χ^2 with these three parameters held fixed and allowing all other parameters to vary. The results are shown in the upper panel of Figure 6. The curves represent detection efficiencies of 25%, 50%, 75%, and 95%. For $q = 0.1$, companions with separation $0.2 \lesssim d \lesssim 6$ are completely excluded by the data because they would produce deviations $\Delta\chi^2 \equiv \chi^2(d, q, \alpha) - \chi^2_{\text{PSPL}} > 60$ that are not observed. However, the effect of planetary companions of mass ratio $q = 10^{-5}$ would hardly be discernible.

Gaudi et al. (2002) discussed a potential shortcoming of this approach: if (as in the present case) u_0 is not well constrained by the data, then it is possible that for the procedure to say that certain planetary configurations are permitted by the data when in fact they are excluded. For example, suppose that the measured impact parameter is $u_0 = 0.00250 \pm 0.00072$ while the actual value is $u_0 = 0.003$. For some value of α , the caustic induced by a planet could lie right along the $u_0 = 0.003$ trajectory, but the minimization routine might nevertheless find a path that lay 5σ ($\Delta\chi^2 = 25$) from this value at $u_0 = 0.006$ and so avoided the planetary caustic but with $\Delta\chi^2 < 60$ (see Fig. 6 and the accompanying text in Gaudi et al. 2002).

To counter this shortcoming, we evaluate the sensitivity at each allowed value of u_0 . Our search of (d, q, u_0) parameter space reveals no planets. The best fit is at $u_0 = 0.002$, $d = 1$, $q = 10^{-3.8}$, but the $\Delta\chi^2$ is only -2.9 , far short of our adopted threshold of $\Delta\chi^2_{\text{thr}} = -60$. We evaluate the efficiency by modifying equation (15) to become

$$\epsilon(d, q; u_0) = \frac{1}{2\pi} \int_0^{2\pi} d\alpha \Theta [\chi^2(d, q, \alpha; u_0) - \chi^2_{\text{PSPL}}(u_0) - \Delta\chi^2_{\text{thr}}], \quad (16)$$

where $\chi^2(d, q, \alpha; u_0)$ and $\chi^2_{\text{PSPL}}(u_0)$ are now evaluated at fixed u_0 . Here, u_0 is defined as the projected separation of the source from the center of the caustic induced by the planetary companion. This is the appropriate generalization from the point-lens case, in which u_0 is the projected separation from the (point-like) caustic at the position of the primary lens. The lower panel of Figure 6 shows 50% contours of detec-

tion efficiency for several values of u_0 that are consistent with the Monte Carlo simulation (see Fig. 5). For comparison, we present the 50% contours of the Albrow et al. (2000) method (*solid*) and of our new method with $u_0 = 0.002$ and $u_0 = 0.004$ (*dashed*) in the inset. Although the difference is small, we find that the previous method of Albrow et al. (2000) tends to overestimate the detection efficiency.

While it is comforting that the magnitude of this effect is small, its sign is somewhat unsettling. Recall that one motivation for integrating over u_0 rather than minimizing with respect to u_0 was that under the latter procedure, the trajectory could "avoid" planetary caustics and underestimate the sensitivity. In the present case, however, this effect is outweighed by the fact that the most probable value of u_0 is increased by taking into account the Monte Carlo compared to the fit to the lightcurve alone. See Figure 5. As discussed in § 1, sensitivity to planets generally decreases with increasing u_0 .

Note that in this particular case, it is only necessary to integrate over u_0 (and not all lightcurve parameters as originally envisaged by Gaudi et al. 2002) because once u_0 is specified, all the other lightcurve parameters are highly constrained (see § 4.2).

One might be concerned about finite-source effects during a planet-caustic crossing. However, we have repeated the calculation including finite-source effects for a variety of (d, q, α) combinations and for various plausible source sizes as determined from Monte Carlo. We find no significant difference in planet detection efficiencies.

6.2. Constraints on Planets

Gravitational microlensing events provide only degenerate information on physical properties of the source and lens except in so far as other higher order effects such as finite-source effects and parallax are detected. However, our new method based on Monte Carlo simulations allows us, for the first time, to break the degeneracy and place constraints on planetary companions in the planet-mass/physical-separation plane, rather than scaling these quantities to the stellar mass and Einstein radius as was done previously.

For a given ensemble of Monte Carlo events with posterior

probabilities $P_k(\mathbf{a}^{\text{phys}})$, the detection efficiency ϵ can be evaluated as a function of the planet mass m and the planet-star projected physical separation r_{\perp} by,

$$\epsilon(r_{\perp}, m) = \frac{\sum_{k=1}^N \epsilon(r_{\perp}/d_{l,k} \theta_{E,k}, m/M_k; u_{0,k}) P(\mathbf{a}^{\text{phys},k})}{\sum_{k=1}^N P(\mathbf{a}^{\text{phys},k})} \quad (17)$$

where N is the number of Monte Carlo events and $\theta_E(M, d_l, d_s)$ is the angular Einstein radius.

Figure 7 shows the resulting detection efficiency with the curves representing contours for $\epsilon = 25\%$, 50% , 75% , and 95% . The left and middle panels show separate detection efficiencies for the MS+BDs, and the remnant stars, respectively. The total efficiency is shown in the right panel. Since remnant stars are more massive than MS+BDs, at fixed planet-star mass ratio, microlensing events by remnant stars probe planets of higher absolute mass. Hence, microlensing is less efficient as a probe of planets of remnants than of MS+BDs at fixed planetary mass.

Because our Galactic model favors substantially lower blending than is implied by the lightcurve alone, the best fit magnitude is reduced from $A = 400$ to $A = 256$. Nevertheless, OGLE-2003-BLG-423 is the highest magnification single-lens event recorded to date. Despite this honor, the detection efficiency is not quite as good as two previous high magnification events, MACHO-98-BLG-35 ($A_{\text{max}} \sim 100$) and OGLE-1999-BUL-35 ($A_{\text{max}} \sim 125$) (Gaudi et al. 2002, see

also Bond et al. 2002). This is because our observations do not cover the peak of the lightcurve nearly as densely as was the case in those two events. Peak coverage is key because the perturbations by planets mostly occur during a small time interval, basically the full width at half maximum around the peak of the event (Rattenbury et al. 2002).

We thank Jean-Philippe Beaulieu, David Bennett, Martin Dominik and Phil Yock for valuable comments on the manuscript. Work at OSU was supported by grants AST 02-01266 from the NSF and NAG 5-10678 from NASA. A. G.-Y. acknowledges support by NASA through Hubble Fellowship grant #HST-HF-01158.01-A awarded by STScI, which is operated by AURA, Inc., for NASA, under contract NAS 5-26555. B.S.G. was supported by a Menzel Fellowship from the Harvard College Observatory. C.H. was supported by the Astrophysical Research Center for the Structure and Evolution of the Cosmos (ARCSEC) of Korea Science & Engineering Foundation (KOSEF) through Science Research Program (SRC) program. Partial support to the OGLE project was provided with the NSF grant AST-0204908 and NASA grant NAG5-12212 to B. Paczyński and the Polish KBN grant 2P03D02124 to A. Udalski. A.U., I.S. and K.Ż. also acknowledge support from the grant ‘‘Subsydium Profesorskie’’ of the Foundation for Polish Science.

REFERENCES

- Albrow, M. D. 2004, *ApJ*, 607, 821
 Albrow, M. D., et al. 1998, *ApJ*, 509, 687
 Albrow, M. D. et al. 2000, *ApJ*, 535, 176
 Albrow, M. D. et al. 2001, *ApJ*, 556, L113
 Bennett, D.P., & Rhie, S.H. 2002, *ApJ*, 574, 985
 Bond, I. A., et al. 2002, *MNRAS*, 333, 71
 European Space Agency, 1997, *The Hipparcos and Tycho Catalogues* (SP-1200; Noordwijk: ESA)
 Gaudi, B. S. & Gould, A. 1997, *ApJ*, 486, 85
 Gaudi, B. S., & Han, C., *ApJ* in press, astro-ph/0403459
 Gaudi, B. S., Han, C. & Gould, A. 2004, in preparation
 Gaudi, B. S., & Sackett, P. D. 2000, *ApJ*, 528, 56
 Gaudi, B. S., et al. 2002, *ApJ*, 566, 463
 Gould, A. 2000, *ApJ*, 535, 928
 Gould, A. 2004, astro-ph/0403506
 Gould, A., & Loeb, A. 1992, *ApJ*, 396, 104
 Griest, K. & Safizadeh, N. 1998, *ApJ*, 500, 37
 Han, C. & Gould, A. 1996, *ApJ*, 467, 540
 Han, C. & Gould, A. 2003, *ApJ*, 592, 172
 Holtzman, J. A., et al. 1998, *ApJ*, 115, 1946
 Rattenbury, N. J., Bond, I. A., Skuljan, J., & Yock, P. C. M. 2002, *MNRAS*, 335, 159
 Rhie, S. H., Becker, A. C., Bennett, D. P., Fragile, P. C., Johnson, B. R., King, L. J., Peterson, B. A., & Quinn, J. 1999, *ApJ*, 522, 1037
 Rhie, S. H. et al. 2000, *ApJ*, 533, 378
 Snodgrass, C., Horne, K., & Tsapras, Y. 2004, *MNRAS* in press, astro-ph/0403387
 Tsapras, Y., Horne, K., Kane, S., & Carson, R. 2003, *MNRAS*, 343, 1131
 Udalski, A. 2003, *Acta Astron.*, 53, 291
 Udalski, A., et al. 2002, *Acta Astron.*, 52, 1
 Yoo, J., et al. 2004, *ApJ*, 603, 139
 Zoccali M., et al. 2000, *ApJ*, 530, 418